Physics and Imaging in Radiation Oncology 14 (2020) 74–81

Contents lists available at ScienceDirect

Physics and Imaging in Radiation Oncology

journal homepage: www.elsevier.com/locate/phro

Clinical microbeam radiation therapy with a compact source: specifications of the line-focus X-ray tube

Johanna Winter[a,b,c,*], Marek Galek[d], Christoph Matejcek[b,e], Jan J. Wilkens[b,c], Kurt Aulenbacher[e,f,g], Stephanie E. Combs[a,b], Stefan Bartzsch[a,b]

[a] Helmholtz Zentrum München GmbH, German Research Center for Environmental Health, Institute of Radiation Medicine, Ingolstädter Landstr. 1, 85764 Neuherberg, Germany
[b] Technical University of Munich, School of Medicine and Klinikum rechts der Isar, Department of Radiation Oncology, Munich, Germany
[c] Technical University of Munich, Physics Department, Garching, Germany
[d] University of Applied Sciences, Department of Electrical Engineering and Information Technology, Munich, Germany
[e] Johannes Gutenberg-Universität Mainz, Institut für Kernphysik, Mainz, Germany
[f] GSI Helmholtzzentrum für Schwerionenforschung, Darmstadt, Germany
[g] Helmholtz-Institut Mainz, Germany

ARTICLE INFO

Keywords:
Microbeam radiation therapy
Line-focus X-ray tube
Compact radiation source
Modular high-voltage supply
Microbeam arc therapy
Equivalent uniform dose

ABSTRACT

Background and purpose: Microbeam radiotherapy (MRT) is a preclinical concept in radiation oncology with arrays of alternating micrometer-wide high-dose peaks and low-dose valleys. Experiments demonstrated a superior normal tissue sparing at similar tumor control rates with MRT compared to conventional radiotherapy. Possible clinical applications are currently limited to large third-generation synchrotrons. Here, we investigated the line-focus X-ray tube as an alternative microbeam source.

Materials and methods: We developed a concept for a high-voltage supply and an electron source. In Monte Carlo simulations, we assessed the influence of X-ray spectrum, focal spot size, electron incidence angle, and photon emission angle on the microbeam dose distribution. We further assessed the dose distribution of microbeam arc therapy and suggested to interpret this complex dose distribution by equivalent uniform dose.

Results: An adapted modular multi-level converter can supply high-voltage powers in the megawatt range for a few seconds. The electron source with a thermionic cathode and a quadrupole can generate an eccentric, high-power electron beam of several 100 keV energy. Highest dose rates and peak-to-valley dose ratios (PVDRs) were achieved for an electron beam impinging perpendicular onto the target surface and a focal spot smaller than the microbeam cross-section. The line-focus X-ray tube simulations demonstrated PVDRs above 20.

Conclusion: The line-focus X-ray tube is a suitable compact source for clinical MRT. We demonstrated its technical feasibility based on state-of-the-art high-voltage and electron-beam technology. Microbeam arc therapy is an effective concept to increase the target-to-entrance dose ratio of orthovoltage microbeams.

1. Introduction

Certain inoperable tumors such as glioblastoma multiforme remain to have poor prognosis, despite advances in modern cancer care. The effectiveness of radiotherapy is limited by radiosensitive organs at risk close to the tumor. The yet preclinical concept of microbeam radiation therapy (MRT) [1] has shown superior normal tissue sparing at similar tumor control rates compared to conventional radiotherapy [2,3] and is therefore promising for treating aggressive tumors. MRT utilizes spatial fractionation [4] of the dose distribution into an array of quasi-parallel, planar photon beams of 25–100 μm width and unconventionally high doses of hundreds of Grays at the target. These high-dose regions (peaks), separated by 100–400 μm, alternate with low-dose areas (valleys). The biological effects of MRT are not fully understood yet [5], and it is still unclear if a spatially fractionated target dose is more efficient than a homogeneous target dose [2]. Nevertheless, authors agree that a low valley dose, a high peak-to-valley dose ratio (PVDR), and steep lateral penumbras from the peaks to the valleys are crucial for sparing healthy tissue [5–7].

Mean photon energies of 100–150 keV give the best compromise

* Corresponding author at: Helmholtz Zentrum München GmbH, German Research Center for Environmental Health, Institute of Radiation Medicine, Ingolstädter Landstr. 1, 85764 Neuherberg, Germany.
E-mail address: johanna.winter@helmholtz-muenchen.de (J. Winter).

https://doi.org/10.1016/j.phro.2020.05.010
Received 27 February 2020; Received in revised form 20 May 2020; Accepted 29 May 2020

between short ranges of secondary electrons, allowing steep lateral penumbras, and shallow depth doses for reaching deep-seated tumors [7–10]. The radiation source needs low divergence and a focal spot smaller than an individual microbeam to maintain the dose pattern and sharp beam penumbras in larger depth in the tissue [11]. A high dose rate, up to kilograys per second, prevents blurring of the microbeam pattern caused by organ motion [7].

These requirements are fulfilled at some third-generation synchrotrons [7]. However, the limited availability, enormous size, and high costs render synchrotrons unfeasible for routine clinical radiotherapy.

For a clinical MRT, compact sources are required. Various concepts have been suggested, including inverse Compton scattering sources [12], carbon nanotube field emission technology [13], and conventional X-ray tube-based sources [14,15]. However, none of the suggested alternatives to synchrotrons achieve dose rates adequate to patient treatments. A strategy that might succeed in sufficiently high dose rates is the line-focus X-ray tube [11].

In this study, we investigated the technical feasibility of the line-focus X-ray tube for clinical application in MRT. State-of-the-art electron accelerators [16,17] provide beam currents of 1 A at 500 keV energy and therefore generate sufficient electron beam power. However, it is challenging to focus beams to a micrometer-sized focal spot. Moreover, such an accelerator requires high-voltage (HV) pulses in the megawatt range for several seconds, which commercially available HV generators struggle to deliver. We investigated the suitability of modular multi-level converters (MMCs) from the high-voltage direct-current transmission technology. Finally, we analyzed the dose distribution of the line-focus X-ray tube and showed that microbeam arc therapy can be a strategy to avoid high beam entrance doses of orthovoltage x-rays.

2. Materials and methods

The line-focus X-ray tube is a modified X-ray tube with two unique features: a strongly eccentric focal spot with a width of tens of micrometers and a high target surface velocity of 200 m s^{-1}. These two features shift the physical characteristics of target heating from the heat conduction limit for conventional X-ray tubes to the heat capacity limit [11]. In the heat capacity limit, the current density can be increased while keeping the focal spot temperature below the target melting point. With these high electron currents, X-ray dose rates of a few hundred Grays per second can be achieved to avoid blurring of the dose pattern due to organ motion. A multislit collimator shapes the uniform radiation field into microbeams. For a clinical application, the line-focus X-ray tube is required to deliver a dose rate of above 100 Gy/s (50 cm from the focal spot) with an acceleration voltage of 600 kV, a power of 1.5 MW, an electron current of 2.5 A, and a focal spot size of 0.05×20 mm^2 [11].

The next subsections build up on these quantities and provide a possible realization of the components and applications. We developed an HV supply, considering its power consumption, energy storage and insulation, and an electron source which meets the demand of a small emittance from the cathode through the quadrupole to the target. The microbeam field was optimized regarding the X-ray spectrum, focal spot size, electron incidence angle, and photon emission angle. Microbeam arc therapy was investigated with a head phantom study.

2.1. High-voltage supply

Due to the low overall efficiency of X-ray tubes in the single-digit percentage range, high dose rates lead to a particularly high power consumption. The HV supply for the line-focus X-ray tube was to be designed for an output power of 2 MW, an output voltage of 600 kV (± 300 kV referred to earth potential), and irradiation times of 5 s with an interval of 1200 s [11]. A commercially available HV supply does not exist for these requirements. Main design challenges of a new supply concept were reduced to the following points:

The high output voltage of the converter affects the usable HV semiconductors, the converter topology and the insulation concept. Modern power semiconductors have a maximum blocking voltage of 6.5 kV so that the system supply cannot be implemented monolithically.

The energy supplier requires a continuous input power since peak loads of 2 MW lead to considerable disturbances in the public grid. The continuous input power requires a buffering, which is typically achieved by batteries. Considering the irradiation intervals, the average power consumption is reduced to approximately 10 kW.

Adjustment options for the voltage amplitude as well as the voltage slope of the converter are necessary as even small parasitic components such as earth capacitance lead to high unintended interferences during the switching event for these high voltages.

A distributed energy storage is beneficial as smaller units are easier to handle in case of malfunction. Using a single rechargeable battery would require considerable constructive and structural precaution.

The design challenges are comparable to those in modern high-voltage direct-current transmission, where they are met by modular multi-level converters (MMC) [18]. An MMC is based on identical units as individually switchable voltage sources. A series connection of these voltage sources can generate high output voltages with low blocking voltage components. For the line-focus X-ray tube, we developed an HV supply concept based on an adapted MMC.

2.2. Electron beam

The HV supply provides the power for the electron source which accelerates and focuses the beam onto the target. The generation of a micrometer-sized focal spot requires high electron beam quality. For the line-focus X-ray tube, in particular the emittance ϵ, a conserved quantity characterizing beam size z and divergence $z' = \mathrm{d}z/\mathrm{d}x$, has to be small. The normalized root mean square (rms) emittance is defined as

$$\epsilon_{\mathrm{rms}} = \gamma\beta\sqrt{\langle z^2\rangle\langle z'^2\rangle - \langle zz'\rangle^2}\,. \tag{1}$$

The dimensionless parameters γ and β are the Lorentz factor and the velocity divided by the speed of light, respectively. $\langle z^2\rangle$ represents the second moment of the z-distribution. Space-charge fields arising from high beam currents and relatively low kinetic energies needed to be incorporated into the electron source development as they defocus the beam and lead to emittance growth.

At the end of the beamline, a quadrupole magnet can form an eccentric beam spot by focusing in one dimension and defocusing in the other. An advantage of the quadrupole is the possibility to vary the spot size.

A first approach to calculate the demanded emittances and beam dimensions upstream of the quadrupole were the K-V-equations [19] which describe space-charge effects on the beam size. In front of the proposed quadrupole, the beam diameter needed to be smaller than 10 mm to avoid the stray field on the periphery of the quadrupole which causes emittance growth. This led to a maximum emittance of 0.2 mm to achieve a focal width of 50 μm assuming a focal length of 11 cm. In addition spherical aberration limits the focal size.

To extract the required currents with a long lifetime and low emittance, thermionic cathodes are the best choice. The normalized rms emittance of a thermionic cathode is given by

$$\epsilon_{\mathrm{rms}} = \frac{d_{\mathrm{cath}}}{4}\sqrt{\frac{k_{\mathrm{B}}T}{m_0c^2}}\,, \tag{2}$$

where d_{cath} is the cathode diameter in the direction of interest, $k_{\mathrm{B}}T$ the thermal energy, and m_0c^2 the electron rest mass energy [20]. A small cathode needs a high temperature for high output currents. The maximum temperature of a barium tungsten dispenser cathode (Type: 411 M) recommended by the manufacturer is 1190°, which results in a

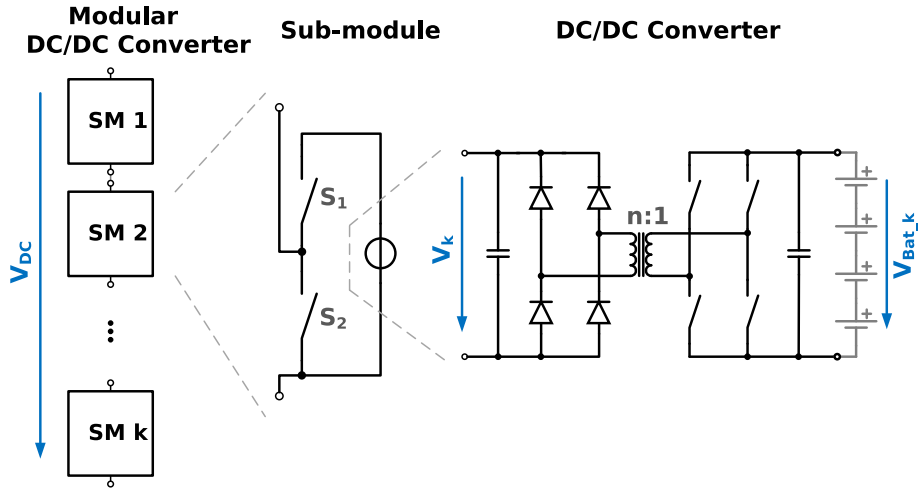

Fig. 1. Modular DC/DC converter setup with distributed energy storage.

current density of 15 A cm^{-2} [21]. For a current of 2.5 A and a circular emission area, the theoretical cathode emittance is thus 0.6 mm.

Optionally, a rectangular cathode can be used with the advantage of a smaller beam size and therefore a sufficiently small emittance in one direction. Nevertheless, a quadrupole is necessary for focus adjustment.

Tracking simulations with CST [22] were performed to find an appropriate design for the electron source. At the electrode structure, electric fields above 10 MV m^{-1} had to be avoided to reduce the risk of electrical breakdown.

2.3. X-ray optimization

At the focal spot, the accelerated electrons hit the target and create a divergent X-ray field which is shaped into microbeams by a multislit collimator. The radiation transport of the line-focus X-ray tube was simulated with Monte Carlo in Geant4 (version 10.4.2, Penelope physics library). A parallel electron beam (200–800 keV) hit the cylindrical tungsten target on the front face in an eccentric Gaussian-shaped focal spot. The spot width was varied between 10 and 500 µm, the spot length between 5 and 40 mm.

The generated x-rays traveled through a 0.8 mm beryllium window, aluminum or copper filters of different thickness, and a microbeam collimator (field size 20 × 20 mm^2, divergent slits of 50 µm × 20 mm [23,24]), which was positioned 50 cm from the focal spot. The absorber thickness of the collimator was adjusted to the maximum photon energy for less than 0.25 % leakage radiation. This resulted in a total tungsten thickness of 7–35 mm depending on the initial electron energy. Attached to the collimator, a water phantom served as detector with a scoring grid of 1 × 1 × 0.005 mm^3.

The investigation of the microbeam dose distribution was separated into the influence of the X-ray spectra, the focal spot size, and the electron incidence angle onto the target as well as the X-ray emission angle. The angles were optimized for maximum energy deposit in water, corresponding to maximum dose rate. At the end, PVDR values achievable with optimal X-ray field parameters are presented.

As a PVDR comparison to state-of-the-art MRT with parallel beams, Geant4 simulations were carried out with parallel X-ray microbeams and the spectrum from the ID17 biomedical beamline at the European Synchrotron Radiation Facility in Grenoble, France. The spectrum at ID17 has a maximum energy of 250 keV and a mean energy of 104 keV [25].

2.4. Microbeam arc therapy

Due to steep depth-dose curves of orthovoltage x-rays, entrance doses are higher than target doses with single-field MRT. To reduce peak entrance doses, we analyzed microbeam arc therapy as a potential MRT application for brain tumor treatments. In Geant4 we simulated a simple spherical head phantom of 70 mm radius with 1 mm water-equivalent skin and 6 mm cortical bone surrounding water-equivalent brain tissue. The water-equivalent tumor was located in the middle of the phantom. Microbeams of 400, 600, and 800 kVp were rotated a full arc (360°) about the phantom with a central rotation axis in z-direction, parallel to the short axis of the microbeams. The long axis of the microbeams was in y-direction, and the beam direction was in x-direction (see Fig. 6a).

To interpret spatially fractionated dose distributions, the calculation of the equivalent uniform dose (EUD) has been suggested [26]. With the EUD concept, inhomogeneous dose distributions are assigned to a homogeneous dose that leads to the same clonogenic cell survival [27].

For a first application of EUD to microbeam arc therapy, we used generic parameters for cell survival in the linear-quadratic model [28] (tumor: $\alpha/\beta = 10\,\mathrm{Gy}$, $\alpha = 0.3\,\mathrm{Gy}^{-1}$ [29,30]; normal brain tissue: $\alpha/\beta = 2\,\mathrm{Gy}$, $\alpha = 0.1\,\mathrm{Gy}^{-1}$ [31]). The dose distribution was normalized to 2.0 Gy valley dose in the tumor region as a typical radiotherapy fraction [30,32].

3. Results

3.1. High-voltage supply

The developed concept of the energy supply in Fig. 1 represents an adapted version of a conventional MMC where the capacitor was replaced by a DC/DC converter. The DC/DC converter boosts the battery voltage into the kilovolt range. The complementary power switches (S_1 and S_2) bridge or insert the sub-module in the module chain: As soon as S_1 is opened, S_2 is closed and the output terminals are short-circuited so that no voltage is added to the main output voltage. In the other case, S_1 is closed and the sub-module voltage V_k is added to the voltage sum of the converter V_{DC}:

$$V_{DC} = \sum_{t=1}^{k} V_k = \sum_{t=1}^{k} n \cdot V_{\mathrm{Bat}_k} \tag{3}$$

This approach allows to accurately set the level and slope of the output voltage even during operation.

To avoid manual handling during the charging process, the batteries are charged through the main DC-link terminals: All modules are bypassed beside the one to be charged. By an automated switching through all modules, a single low-voltage power supply can charge the batteries. A slight adaption of the sub-module DC/DC converter is

necessary to enable a bidirectional power flow.

As seen in Fig. 2, the design of the sub-modules is based on a planar transformer with its windings integrated into the printed circuit board (PCB). To reduce the insulation distances, the cooler is referenced to the negative pole of the battery voltage and to half the output voltage. Thus no voltage of the module exceeds 1 kV in relation to the cooler. The specifications of each of the 300 sub-modules are the following: 6.67 kW output power, 2 kV output voltage, 3.33 A output current, and 12·3.7 V battery voltage.

The presented HV setup can safely supply the electron source with sufficient power to generate high electron beam currents and thus high X-ray dose rates of above 100 Gy/s.

3.2. Electron beam

The result of the electron source setup optimized with CST is shown in Fig. 3. To suppress emittance growth due to space-charge fields of the electron beam, a high gradient of the accelerating electric field was mandatory. This high gradient was achieved by a small distance between cathode and anode. A pierce electrode focused the electron beam to a size small enough to avoid the stray field of the quadrupole. An acceleration tube further accelerated and focuses the beam by several electrodes with increasing electric potential. Behind the acceleration tube, a quadrupole magnet formed an eccentric beam spot. The simulations showed that the achievable emittance was smaller with a rectangular than with a circular cathode.

3.3. X-ray optimization

3.3.1. Influence of the X-ray spectra

For highest PVDR and steepest penumbras, the electron energy should be 300–400 keV, as seen in Fig. 4a. In simulations, beams of lower energy had a steeper depth-dose curve and a lower PVDR in depth. With higher energies, secondary electrons scattered from the peak farther into the valley region which increased the valley dose, decreased the PVDR, and increased the penumbras and full width at half maximum (FWHM).

For 300 and 400 keV electrons, a filter of 0.4 mm copper (resulting in 97 and 109 keV mean photon energy, respectively) was a good compromise between high PVDR, steep penumbras, shallow depth dose, and high relative output.

3.3.2. Influence of the focal spot size

The Gaussian standard deviations of the focal spot should not be larger than an individual collimator slit, resulting in a maximum spot size of 50 μm × 20 mm for the used collimator. A spot wider than 50 μm resulted in a lower PVDR (see Fig. 4b) and broader penumbras and FWHM. A further reduction in spot width had no impact on the microbeam dose distribution or PVDR, which can be seen from the comparison to a point source in Fig. 4b. Longer spots only increased the longitudinal penumbras.

3.3.3. Influence of the incidence and emission angles

The photon energy deposit was maximum for small electron incidence angles onto the target and exhibited a shoulder region for small photon emission angles (polar angle θ), see Fig. 5. Regarding the azimuthal angle ϕ, the photons were emitted uniformly. Taken an incidence angle of 0° or 10°, emission angles between 0° and 50° resulted in a decrease of less than 5% of the maximum efficiency.

3.3.4. Achievable PVDR values

With the requirements described in 3.3.1 to 3.3.3, a PVDR above 30 was achieved in 10 mm (above 20 in 40–100 mm) water depth for single-field MRT (see Fig. 4a and 4b). The PVDR decreased with depth up to 50 mm due to increased Compton scattering into the valleys. Beyond 50 mm, the PVDR remained constant as peak and valley dose decreased at the same rate. At the rear end of the phantom, the PVDR increased due to less backscattering.

The simulations with parallel microbeams with the ID17 spectrum led to a PVDR of 35 in 10 mm (25 in 40–100 mm) water depth.

3.4. Microbeam arc therapy

With microbeam arc therapy, the peak entrance dose to the cranial bone and to normal brain tissue was considerably decreased and spread over the whole head phantom in x- and y-direction (see Figs. 6a and 6b). Thereby, the tumor peak dose in the center of the phantom decreased by less than 1%.

The central tumor region (x = 70 mm) exhibited a clear peak-valley dose profile as known from single-field MRT as seen in Fig. 6c. The region of highest dose on the periphery of the field (x = 60 mm) was considerably smaller and spread out in z already at few millimeters off the central axis due to field divergence.

Normalized to 2 Gy valley dose, a lower electron energy led to higher dose in the peak regions (see Fig. 6d). In the target center, the PVDR was the same as for single-field MRT in 80 mm water depth[1]: 20, 16, and 12 for 400 keV, 600 keV, and 800 keV, respectively. The peak entrance dose decreased with higher electron energy due to shallower depth-dose curves. For the single field, the target-to-entrance peak dose ratios were 0.059, 0.074, and 0.083; for the rotated field, they were 2.2, 2.8, and 3.1 for 400, 600, and 800 keV electrons, respectively. The gain in target-to-entrance dose ratio by the use of rotation was 37–38, independent of energy.

Fig. 6e shows the EUD distribution for the head phantom with 1 mm^3 voxel size. The EUD approximately followed the valley dose with an offset (see Fig. 6f).

4. Discussion

Essential requirements for microbeam treatments are a sufficiently high dose rate and an adequate PVDR. In order to use the line-focus X-ray tube for MRT, we developed concepts for an HV supply and an electron source. For a high PVDR, the eccentric focal spot must be smaller than the microbeam cross section. Microbeam arc therapy can increase the target-to-entrance dose ratio of orthovoltage x-rays, while keeping the PVDR in the phantom center similar to single-field MRT. Microbeam arc therapy can be interpreted by EUD.

The presented modular HV supply fulfills the requirements for high dose rates. Due to the redundancy by many modules, the setup represents a reliable [33] and universal voltage source also for other pulsed applications such as computed tomography or electron cyclotron resonance heating. For high dose rates, the angle-dependent X-ray output power from the target is essential. The electron beam incidence angle should therefore be roughly perpendicular (0–10°).

Regarding the focal spot size, especially its width is critical for successful MRT [11]. Analytical calculations of the electron beam showed the possibility of achieving the required spot size. In simulations, the geometry of the cathode, the pierce electrode, the anode, and the quadrupole magnet must be optimized. Additionally, we will consider an increased acceleration gradient and cathode types other than barium tungsten dispenser cathodes, e.g. lanthanum hexaboride cathodes which have a higher electron yield per area and thus a smaller emitting area. Despite the higher operation temperature of approximately 1800°, this promises achieving a smaller emittance. Changes in position or size of the focal spot, that may result from intensity fluctuations of the thermionic cathode or from target vibrations, must be kept to a minimum.

For the line-focus X-ray tube, we simulated PVDR values

[1] The phantom center was in 80 mm water-equivalent depth considering the relative density of 1.7 for cortical bone.

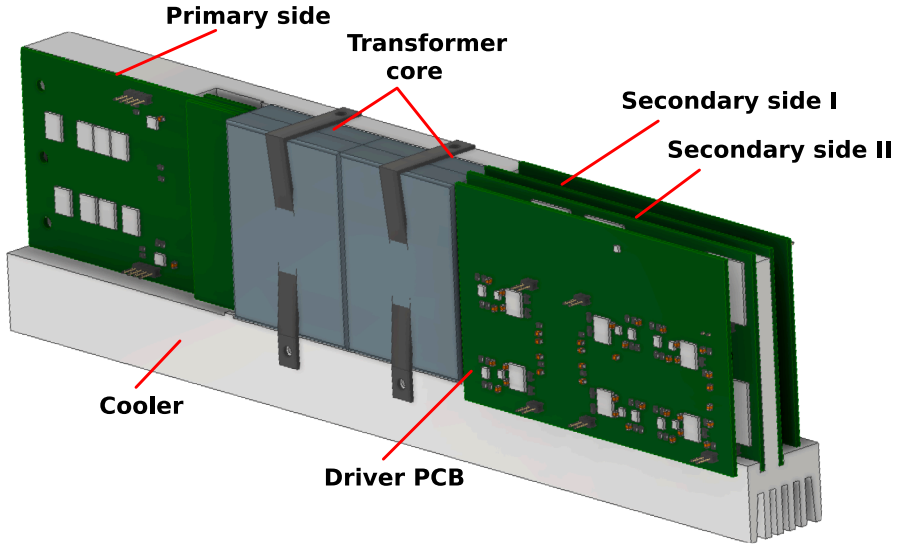

Fig. 2. Sub-module based on a planar transformer.

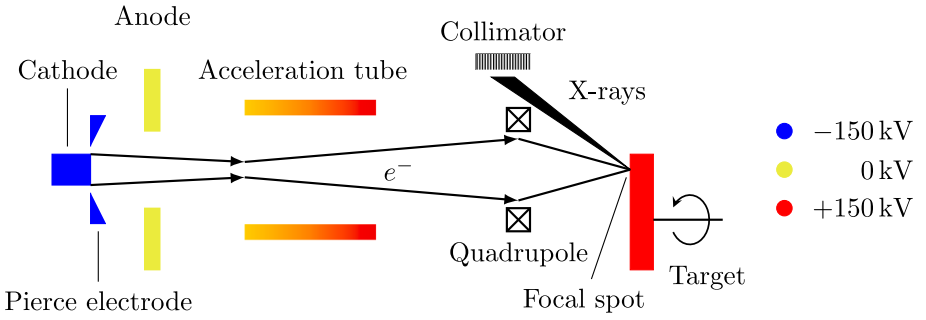

Fig. 3. Schematic of the electron source with the divergent X-ray field. Simulations of the electron beam from the cathode to the focal spot were carried out in CST. Simulations of the X-ray production at the front face of the rotating cylindrical target and the X-ray transport through the collimator with divergent slits were carried out in Geant4. The long axis of the electron beam is in radial target direction.

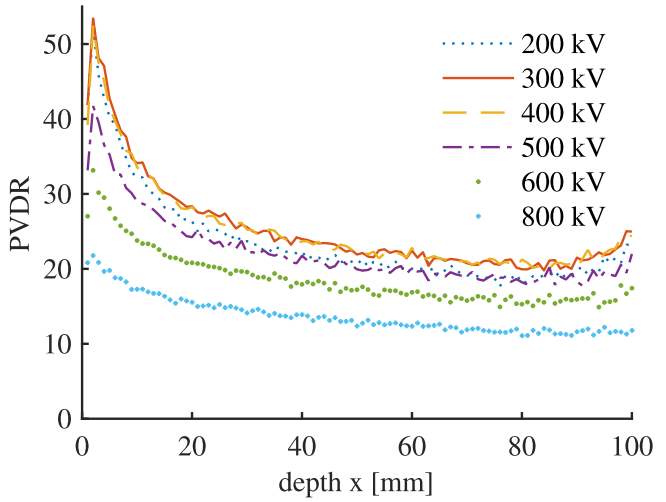

Fig. 4a. Mean peak-to-valley dose ratios (PVDR) for different electron acceleration voltages. The spot was 20 mm long and 50 µm wide. The x-rays were filtered by 0.8 mm beryllium and 0.4 mm copper. The acceleration voltage should be 300–400 kV.

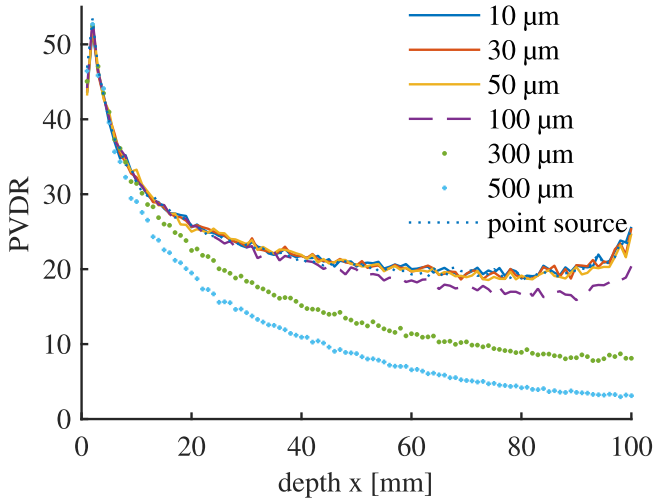

Fig. 4b. Mean peak-to-valley dose ratios (PVDR) for different focal spot widths. The spot was 20 mm long and the x-rays filtered by 0.8 mm beryllium and 0.4 mm copper. The acceleration voltage was 225 kV. The spot width should be smaller or equal to the collimator slit width (50 µm).

comparable to those measured with same field size of 20 × 20 mm^2 at the ID17 [34] where MRT experiments have been successfully performed [2,35,36]. The simulations with parallel microbeams for the line-focus X-ray tube led to PVDR values that were 20% higher in 40–100 mm water depth, which was reasonable considering the missing field divergence. The PVDR trend over depth (as in Fig. 4a and 4b) has been observed before for parallel microbeams [34]. We confirmed an optimal mean photon energy of approximately 100 keV [8,9]. However for clinical treatments of e.g. brain tumors, higher mean energies might be required [7]. A higher energy leads to deeper penetration and a higher target-to-entrance dose ratio which better spares healthy tissue at the same tumor dose.

For further healthy tissue sparing, microbeam arc therapy, similar to conventional arc therapy, is useful for clinical MRT. With the same

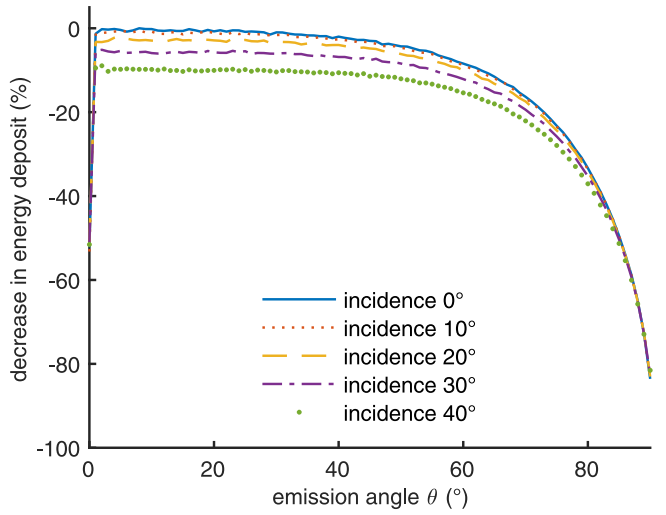

Fig. 5. Emission angle-dependent, integrated dose to a water phantom for 300 keV electrons with different electron incidence angles.

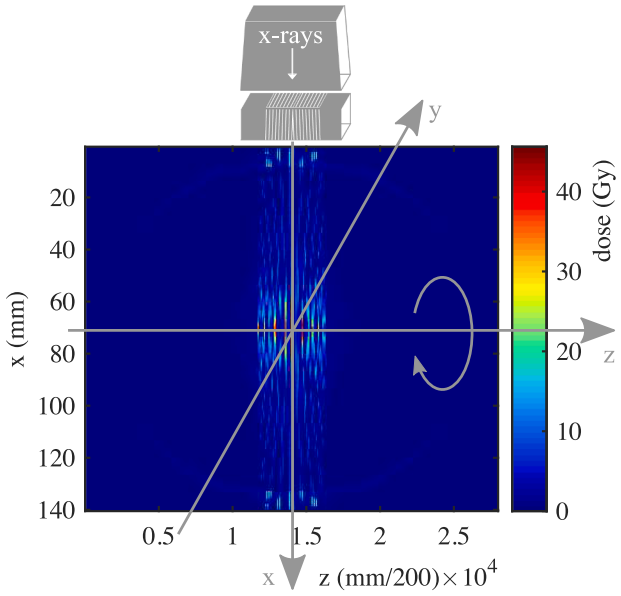

Fig. 6a. Dose distribution in the head phantom with microbeam arc therapy (400 kV) with schematic of the microbeam orientation. The dose distribution was symmetric about the z-axis and normalized to 2 Gy valley dose.

objective of lower peak entrance doses, microbeam multi-port irradiations with a limited number of incidence angles [13,37–40] and a spiralMRT [41] have been suggested. In contrast to most published concepts, our method entails a spatially fractionated dose not only to beam entrance regions but also to the tumor which might further widen the therapeutic window [2].

Microbeam arc therapy generated complex dose distributions with intersecting peaks of varying dose. Currently it is impossible to predict the biological or clinical effect of such beam geometries. The EUD concept was used as an approach to translate the dose distribution of microbeam arc therapy into conventional radiotherapy dose. As the EUD followed the trend of the valley dose, it confirms the observation that normal tissue toxicity depends primarily on the valley dose [2,5,6].

Another medical application of the line-focus X-ray tube might be phase contrast imaging [11]. An additional X-ray exit window at a shallow angle can make the focal spot appear narrower. The very narrow spot together with high dose rates results in a high intensity, spatially coherent beam required for phase contrast imaging [42]. The

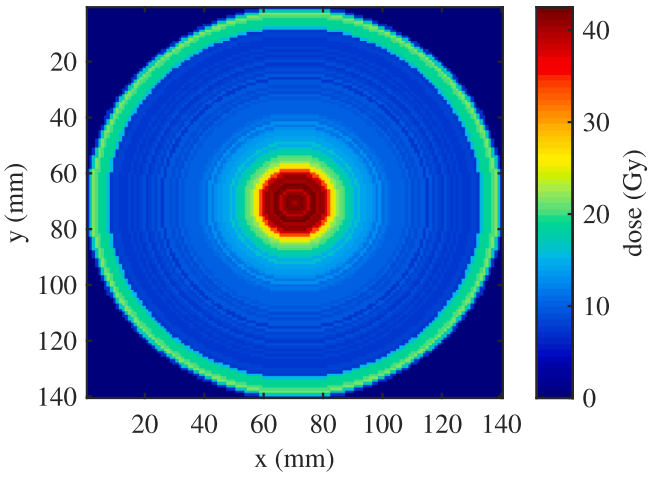

Fig. 6b. Dose distribution in the center peak.

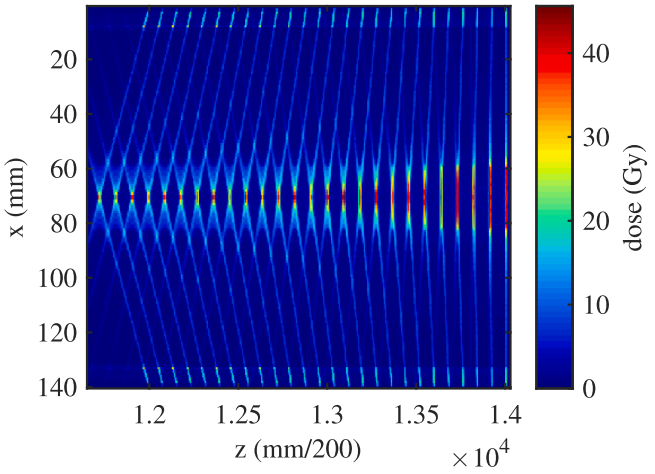

Fig. 6c. Field divergence caused a complex dose distribution.

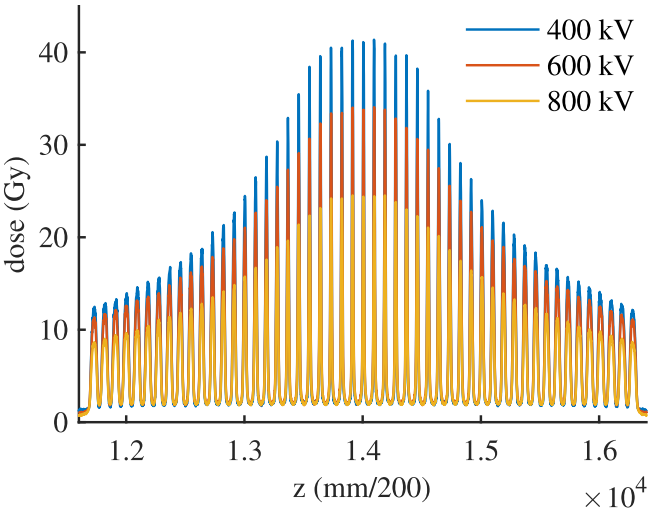

Fig. 6d. Dose profiles at the center of x and y (averaged over 12 mm in x and y).

decrease in dose rate is tolerable for imaging applications.

In conclusion, our simulations demonstrated that the line-focus X-ray tube has great potential as a radiation source for clinical application of MRT. We developed concepts for the high-voltage supply and electron source to deliver high X-ray dose rates from an eccentric electron beam. The compact source can achieve PVDR values comparable to

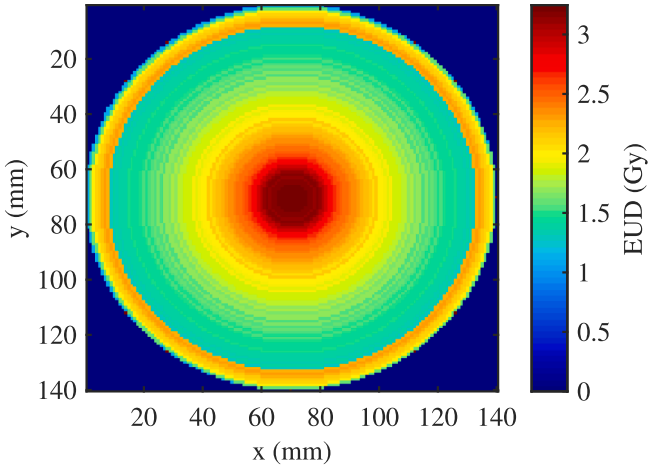

Fig. 6e. Equivalent uniform dose (EUD) distribution.

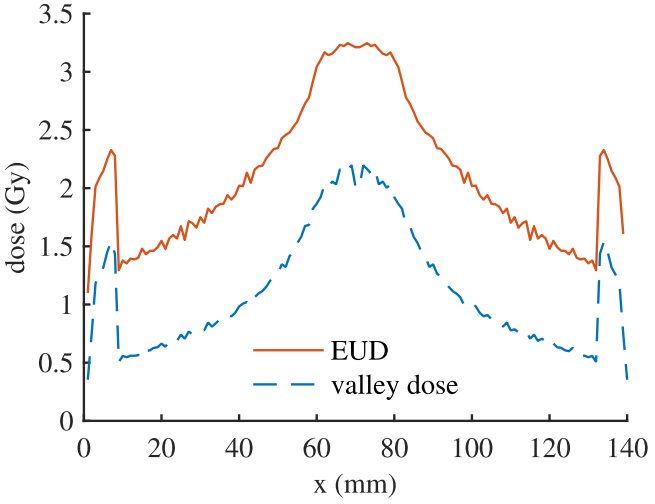

Fig. 6f. Comparison of EUD to central valley dose (valley dose averaged over 0.2mm).

those of successful preclinical MRT experiments and the presented concepts should be experimentally validated.

Declaration of Competing Interest

The authors declare that they have no known competing financial interests or personal relationships that could have appeared to influence the work reported in this paper.

Acknowledgments

This work was supported by the German Research Foundation (Deutsche Forschungsgemeinschaft) through the Emmy Noether Programme with Grant No. 416790481 and the research grant 389238549.

References

[1] Slatkin DN, Spanne PO, Dilmanian FA, Sandbora M. Microbeam radiation therapy. Med Phys 1992;19(6):1395–400. https://doi.org/10.1118/1.596771.
[2] Bouchet A, Bräuer-Krisch E, Prezado Y, El Atifi M, Rogalev L, Le Clec'h C, et al. Better efficacy of synchrotron spatially microfractionated radiation therapy than uniform radiation therapy on glioma. Int J Radiat Oncol Biol Phys 2016;95(5):1485–94. https://doi.org/10.1016/j.ijrobp.2016.03.040.
[3] Smyth LML, Donoghue JF, Ventura JA, Livingstone J, Bailey T, Day LRJ, et al. Comparative toxicity of synchrotron and conventional radiation therapy based on total and partial body irradiation in a murine model. Sci Rep 2018;8(1):1–11. https://doi.org/10.1038/s41598-018-30543-1.
[4] Mohiuddin M, Fujita M, Regine WF, Megooni AS, Ibbott GS, Ahmed MM. High-dose spatially-fractionated radiation (GRID): A new paradigm in the management of advanced cancers. Int J Radiat Oncol Biol Phys 1999;45(3):721–7. https://doi.org/10.1016/S0360-3016(99)00170-4.
[5] Smyth LML, Senthi S, Crosbie JC, Rogers PAW. The normal tissue effects of microbeam radiotherapy: What do we know, and what do we need to know to plan a human clinical trial? Int J Radiat Biol 2016;92(6):302–11. https://doi.org/10.3109/09553002.2016.1154217.
[6] Bazyar S, Inscoe CR, Benefield T, Zhang L, Lu J, Zhou O, et al. Neurocognitive sparing of desktop microbeam irradiation. Radiat Oncol 2017;12(1):127. https://doi.org/10.1186/s13014-017-0864-2.
[7] Bartzsch SH, Corde S, Crosbie JC, Day LRJ, Donzelli M, Krisch M, et al. Technical advances in X-ray microbeam radiation therapy. Phys Med Biol 2020;65(2):02TR01. https://doi.org/10.1088/1361-6560/ab5507.
[8] Spiga J, Siegbahn EA, Bräuer-Krisch E, Randaccio P, Bravin A. The GEANT4 toolkit for microdosimetry calculations: application to microbeam radiation therapy (MRT). Med Phys 2007;34(11):4322–30. https://doi.org/10.1118/1.2794170.
[9] Donzelli M, Bräuer-Krisch E, Oelfke U, Wilkens JJ, Bartzsch S. Hybrid dose calculation: a dose calculation algorithm for microbeam radiation therapy. Phys Med Biol 2018;63(4). https://doi.org/10.1088/1361-6560/aaa705. 045013.
[10] Siegbahn EA, Stepanek J, Bräuer-Krisch E, Bravin A. Determination of dosimetrical quantities used in microbeam radiation therapy (MRT) with Monte Carlo simulations. Med Phys 2006;33(9):3248–59. https://doi.org/10.1118/1.2229422.
[11] Bartzsch S, Oelfke U. Line focus x-ray tubes—a new concept to produce high brilliance x-rays. Phys Med Biol 2017;62(22):8600–15. https://doi.org/10.1088/1361-6560/aa910b.
[12] Jacquet M, Suortti P. Radiation therapy at compact Compton sources. Phys Med 2015;31(6):596–600. https://doi.org/10.1016/j.ejmp.2015.02.010.
[13] Schreiber EC, Chang SX. Monte Carlo simulation of a compact microbeam radiotherapy system based on carbon nanotube field emission technology. Med Phys 2012;39(8):4669–78. https://doi.org/10.1118/1.4728220.
[14] Esplen NM, Chergui L, Johnstone CD, Bazalova-Carter M. Monte Carlo optimization of a microbeam collimator design for use on the small animal radiation research platform (SARRP). Phys Med Biol 2018;63(17). https://doi.org/10.1088/1361-6560/aad7e2. 175004.
[15] Bartzsch S, Cummings C, Eismann S, Oelfke U. A preclinical microbeam facility with a conventional x-ray tube. Med Phys 2016;43(12):6301–8. https://doi.org/10.1118/1.4966032.
[16] Asaka T, Ego H, Hanaki H, Hara T, Hasegawa T, Hasegawa T, et al. Low-emittance thermionic-gun-based injector for a compact free-electron laser. Phys Rev Accel Beams 2017;20(8):80702. https://doi.org/10.1103/PhysRevAccelBeams.20.080702.
[17] Kittimanapun K, Dhammatong C, Juntong N, Phacheerak W, Phanak M. Low Emittance Thermionic Electron Gun at SLRI. 9th Int Part Acc Conf (IPAC 2018), Vancouver, BC, Canada 2018:4509–11. https://doi.org/10.18429/JACoW-IPAC2018-THPMK088. THPMK088.
[18] Lesnicar A, Marquardt R. An innovative modular multilevel converter topology suitable for a wide power range. IEEE Bologna Power Tech Conf Proc 2003;3:6. https://doi.org/10.1109/PTC.2003.1304403.
[19] Hinterberger F. Physik der Teilchenbeschleuniger und Ionenoptik. Springer; 2008.
[20] Bazarov IV, Dunham BM, Li Y, Liu X, Ouzounov DG, Sinclair CK, et al. Thermal emittance and response time measurements of negative electron affinity photocathodes. J Appl Phys 2008;103(5). https://doi.org/10.1063/1.2838209.
[21] Cronin JL. Modern dispenser cathodes. IEE Proc/Solid State Electron Devices 1981;128:19–32. https://doi.org/10.1049/ip-i-1.1981.0012.
[22] Computer Simulation Technology. CST Studio Suite. http://www.cst.com/; 2018.
[23] Treibel F, Wilkens JJ, Combs SE, Bartzsch S. PV-106 An optimized compact microbeam source for preclinical studies. Radiother Oncol 2019;133:S56–7. https://doi.org/10.1016/S0167-8140(19)30526-2.
[24] Flynn S, Price T, Allport PP, Silvestre Patallo I, Thomas R, Subiel A, et al. Evaluation of a pixelated large format CMOS sensor for x-ray microbeam radiotherapy. Med Phys 2020;47(3):1305–16. https://doi.org/10.1002/mp.13971.
[25] Crosbie JC, Fournier P, Bartzsch S, Donzelli M, Cornelius I, Stevenson AW, et al. Energy spectra considerations for synchrotron radiotherapy trials on the ID17 biomedical beamline at the European Synchrotron Radiation Facility. J Synchrotron Radiat 2015;22(4):1035–41. https://doi.org/10.1107/S1600577515008115.
[26] Meyer J, Stewart RD, Smith D, Eagle J, Lee E, Cao N, et al. Biological and dosimetric characterisation of spatially fractionated proton minibeams. Phys Med Biol 2017;62(24):9260–81. https://doi.org/10.1088/1361-6560/aa950c.
[27] Niemierko A. Reporting and analyzing dose distributions: A concept of equivalent uniform dose. Med Phys 1997;24(1):103–10. https://doi.org/10.1118/1.598063.
[28] Fowler JF. The linear-quadratic formula and progress in fractionated radiotherapy. Br J Radiol 1989;62(740):679–94. https://doi.org/10.1259/0007-1285-62-740-679.
[29] Jones LC, Hoban PW. Treatment plan comparison using equivalent uniform biologically effective dose (EUBED). Phys Med Biol 2000;45(1):159–70. https://doi.org/10.1088/0031-9155/45/1/311.
[30] Joiner M, van der Kogel A. Basic Clinical Radiobiology. 4th ed. CRC Press; 2009.
[31] Krämer M, Scholz M. Treatment planning for heavy-ion radiotherapy: calculation and optimization of biologically effective dose. Phys Med Biol 2000;45(11):3319–30. https://doi.org/10.1088/0031-9155/45/11/314.
[32] Barani IJ, Larson DA. Radiation therapy of glioblastoma. Cancer Treat Res 2015;163:49–73. https://doi.org/10.1007/978-3-319-12048-5_4.
[33] Cottet D, Agostini F, Gradinger T, Velthuis R, Wunsch B, Baumann D, et al.

Integration technologies for a medium voltage modular multi-level converter with hot swap capability. IEEE Energy Convers Congress Exposition (ECCE) 2015:4502–9. https://doi.org/10.1109/ECCE.2015.7310295.

[34] Martínez-Rovira I, Sempau J, Prezado Y. Development and commissioning of a Monte Carlo photon beam model for the forthcoming clinical trials in microbeam radiation therapy. Med Phys 2011;39(1):119–31. https://doi.org/10.1118/1.3665768.

[35] Serduc R, Bouchet A, Bräuer-Krisch E, Laissue JA, Spiga J, Sarun S, et al. Synchrotron microbeam radiation therapy for rat brain tumor palliation – influence of the microbeam width at constant valley dose. Phys Med Biol 2009;54(21):6711–24. https://doi.org/10.1088/0031-9155/54/21/017.

[36] Miura M, Blattmann H, Bräuer-Krisch E, Bravin A, Hanson AL, Nawrocky MM, et al. Radiosurgical palliation of aggressive murine SCCVII squamous cell carcinomas using synchrotron-generated X-ray microbeams. Br J Radiol 2006;79(937):71–5. https://doi.org/10.1259/bjr/50464795.

[37] Dilmanian FA, Zhong Z, Bacarian T, Benveniste H, Romanelli P, Wang R, et al. Interlaced x-ray microplanar beams: a radiosurgery approach with clinical potential. Proc Natl Acad Sci USA 2006;103(25):9709–14. https://doi.org/10.1073/pnas.0603567103.

[38] Serduc R, Bräuer-Krisch E, Siegbahn EA, Bouchet A, Pouyatos B, Carron R, et al. High-precision radiosurgical dose delivery by interlaced microbeam arrays of high-flux low-energy synchrotron x-rays. PLoS ONE 2010;5(2). https://doi.org/10.1371/journal.pone.0009028. e9028.

[39] Hadsell M, Cao G, Zhang J, Burk L, Schreiber T, Schreiber E, et al. Pilot study for compact microbeam radiation therapy using a carbon nanotube field emission micro-CT scanner. Med Phys 2014;41(6Part1). https://doi.org/10.1118/1.4873683. 061710.

[40] Bräuer-Krisch E, Requardt H, Régnard P, Corde S, Siegbahn EA, Le Duc G, et al. New irradiation geometry for microbeam radiation therapy. Phys Med Biol 2005;50(13):3103–11. https://doi.org/10.1088/0031-9155/50/13/009.

[41] Donzelli M, Oelfke U, Brauer-Krisch E. Introducing the concept of spiral microbeam radiation therapy (spiralMRT). Phys Med Biol 2019;64(6). https://doi.org/10.1088/1361-6560/aaff23. 065005.

[42] Pfeiffer F, Weitkamp T, Bunk O, David C. Phase retrieval and differential phase-contrast imaging with low-brilliance X-ray sources. Nat Phys 2006;2(4):258–61. https://doi.org/10.1038/nphys265.